Inorganic Chemistry

Article

pubs.acs.org/IC

Tuning Excited States of Bipyridyl Platinum(II) Chromophores with π-Bonded Catecholate Organometallic Ligands: Synthesis, Structures, TD-DFT Calculations, and Photophysical Properties

Jamal Moussa,[†,‡] Lise-Marie Chamoreau,[†,‡] Alessandra Degli Esposti,[§] Maria Pia Gullo,[§] Andrea Barbieri,*[,§] and Hani Amouri*[,†,‡]

[†]Sorbonne Universités, UPMC Univ Paris 06, Université Pierre et Marie Curie and [‡]CNRS, Centre National de la Recherche Scientifique, Institut Parisien de Chimie Moléculaire (IPCM) UMR 8232, 4 place Jussieu, 75252 Paris cedex 05, France

[§]Istituto per la Sintesi Organica e la Fotoreattività (ISOF), Consiglio Nazionale delle Ricerche (CNR), Via Gobetti 101, 40129 Bologna BO, Italy

Supporting Information

ABSTRACT: A series of bipyridyl (bpy) Pt(II) complexes with π-bonded catecholate (cat) $[(bpy)Pt(L_M)][BF_4]_n$ (**2**–**5**) (L_M = Cp*Rh(cat), n = 2; Cp*Ir(cat), n = 2; Cp*Ru(cat), n = 1; and (C_6H_6)Ru(cat), n = 2) were prepared and fully characterized. The molecular structures of the four compounds were determined and showed that the solid-state packing is different and dependent on the π-bonded catecholate unit. For instance, while the (bpy)Pt(II) complexes **2** and **3** with rhodium and iridium catecholates did not show any Pt···Pt interactions those with the ruthenium catecholates **4** and **5** showed the presence of Pt···Pt and π–π interactions among individual units and generated one- and two-dimensional supramolecular chains. The photophysical properties of these compounds **2**–**5** were investigated and showed that all compounds are luminescent at low temperature, in contrast to the well-known parent compound $[(C_6H_4O_2)Pt(bpy)]$ (**1**), which is weakly luminescent at 77 K. Time-dependent density functional theory studies are advanced to explain this difference in behavior and to highlight the role of the π-bonded catecholate system.

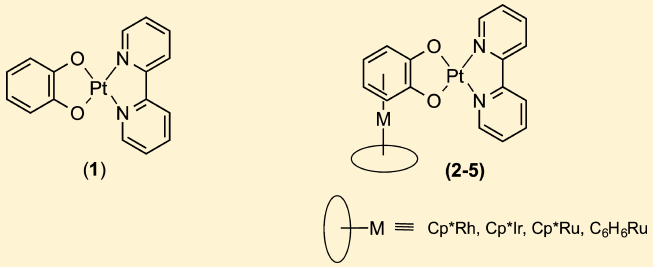

INTRODUCTION

Polypyridyl platinum(II) complexes have attracted much attention in recent decades because of their high performances in various photonic applications[1] such as OLEDs,[2] photocatalysis,[3] hydrogen production,[4] and biological imaging.[5] Unlike their d^6 counterparts such d^8 complexes are coordinatively unsaturated and, hence, allow additional reactions to occur such as self- and cross-quenching,[6] photoreactivity,[7] and photocatalysis. However, Pt(II) complexes with diimine ligands are often nonluminescent in solution at room temperature (rt) due to the presence of low-lying metal-centered d–d states, which leads to efficient nonradiative deactivation.[8] On the other hand efforts were devoted to the development of emissive Pt(II) complexes with dimine ligands by introducing strongly donating ligands to push the energy of the d–d states to higher levels. For instance strong ligand field groups such as acetylides[9] and cyanides[10] were successfully introduced. We also note that complexes with benzoquinone-type ligands were extensively studied because they show rich electrochemical behavior imparted from the dioxolene units, which are known to act as noninnocent ligands.[11] Nevertheless, there are only relatively few catecholate (cat) complexes of Pt(II) known,[12] and only recently the photophysical properties of Pt(II) heteroleptic complexes based on mixed dioxolene and diimine ligands were investigated.[8,13]

Our group has shown that organometallic moieties and in particular "Cp*M" (Cp* = pentamethyl cyclopentadienyl, M = Ru, Rh, and Ir) can stabilize reactive intermediates by modifying their electronic properties.[14] More recently we demonstrated that π-bonded complexes of *o*-quinone $[Cp^*M(C_6H_4O_2)]^n$ (n = 0, M = Rh, Ir; n = −1, M = Ru) can be used as bidentate ligands L_M to prepare luminescent octahedral complexes of the type $[(bpy)_2Ru(L_M)]$.[15] Indeed the catecholate organometallic ligand modifies profoundly the photophysical properties of the ruthenium chromophores and makes them panchromatic absorbers that also act as red and near-infrared emitters.[16] Thus, we decided to investigate the effect of our π-bonded quinonoid ligands on (diimine) Pt(II) chromophores.

In this Paper, we prepared a novel family of π-bonded catecholate complexes of (bpy)Pt(II) (**2**–**5**) (see Chart 1) including four X-ray molecular structures. The novel complexes (**2**–**5**) were found to be emissive and unlike the free metal (diimine)Pt(II) catecholate complex (**1**). Furthermore, the

Received: January 29, 2014
Published: June 10, 2014

   dx.doi.org/10.1021/ic500232w | *Inorg. Chem.* 2014, 53, 6624–6633

Chart 1. Schematic Drawings. (a) Reported Catecholate (bpy)Pt(II) (1). (b) The Novel Phosphorescent (bpy)Pt(II) Complexes (2−5) with π-Bonded Catecholate Ligands

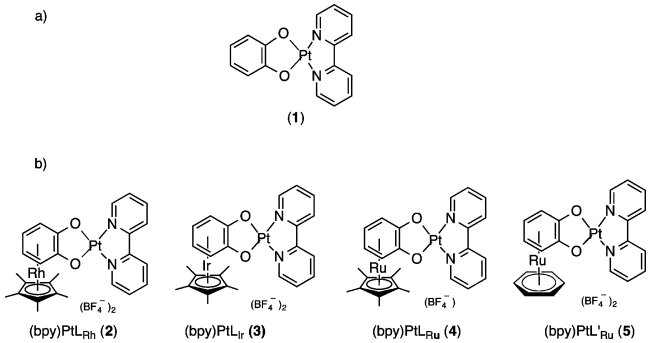

effect on the luminescence properties induced by the organometallic fragment Cp*M (M = Rh, Ru, Ir) or (C_6H_6)Ru π-bonded to catechol is finely tuned. Time-dependent density functional theory (TD-DFT) studies are also advanced to explain the origin of the luminescent properties displayed by our compounds (Chart 1). These results are unprecedented and contribute to the preparation of a novel family of luminescent (bpy)Pt(II) complexes for various applications.

RESULTS AND DISCUSSION

Synthesis and Characterization. The synthesis of the novel compounds $[(bpy)Pt(L_M)][BF_4]_n$ (**2−5**) was achieved through selective π-complexation of the catecholate ring of $[(bpy)Pt(cat)]$[17] (**1**) by the electrophilic Cp*M or C_6H_6Ru moieties according to Scheme 1. Interestingly the organometallic fragment is placed only at the catecholate ring, while it remains coordinated to the platinum center through the oxygen atoms. The target compounds are obtained in good to high yields and were fully characterized including their single-crystal X-ray analysis. For instance ^{1}H NMR of compound $[(bpy)Pt(L_{Rh})][BF_4]_2$ (**2**) in CD_3CN exhibits a singlet at δ 2.07 ppm attributed to the coordinated Cp* ligand and a multiplet at δ 6.27 ppm attributed to the catecholate protons. Furthermore, we observe the presence of a set of signals at δ 7.75 ppm, 8.28, 8.36, and 8.78 ppm attributed to the bpy ligand (see Experimental Section). The infrared spectrum shows a broad band at 1025 cm^{-1} for the BF_4 anion and a weak band at 1613 cm^{-1} for the carbonyl stretching. All other compounds show similar spectroscopic features; we note however, that for complexes **3−5**, two multiplets were observed for the catecholate protons (see Experimental Section). In addition the structures of all compounds were ascertained by single-crystal X-ray diffraction studies, and the results are discussed in the next section.

Scheme 1. Synthesis of the Novel π-Bonded Catecholate Complexes 2−5

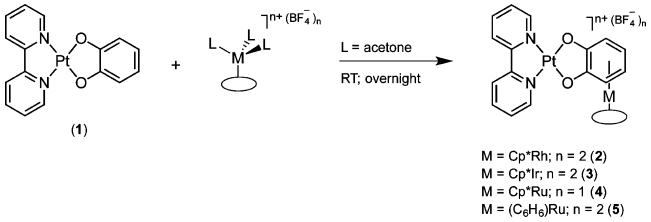

X-ray Molecular Structures of 2−5. Crystals of the above compounds convenient for an X-ray diffraction study were grown at rt by slow diffusion of diethyl ether into solutions of the compounds in acetonitrile. Table 1 summarizes experimental and structure refinement parameters for compounds **2−5**; selected bond lengths and angles are given in Supporting Information, Table S1. The X-ray structural data of complexes **2−5** confirmed the spectroscopic analyses. For instance the structures of both compounds $[(bpy)Pt(L_M)][BF_4]_2$ (**2−3**) displaying a π-bonded catecholate with Cp*M moiety (M = Rh, Ir) showed similar structural features (see Figure 1). In each case one can notice a platinum center chelated by two nitrogen centers of a bpy ligand and also through oxygen centers of catecholate unit. Moreover, the catechol ring is π-coordinated to an organometallic fragment (Cp*M, M = Rh (**2**); M = Ir (**3**)). We also notice the Pt(bpy) moiety leans toward the Cp*M unit with the hinge angle θ between the plane containing Pt(bpy) and the catecholate unit of 8.1° for **2** and 8.45° for **3**, respectively. Analysis of bond lengths and angles revealed that geometry around the platinum center is slightly distorted square planar with Pt−N and Pt−O bond lengths in the range of 1.96−1.98 Å and 1.99−2.02 Å (Supporting Information, Table S1). These values are comparable to those reported for related compounds but without a π-bonded system.[13] Examination of the packing system did not show any Pt···Pt interaction among individual units.

The ruthenium counterparts $[(bpy)Pt(L_{Ru})][BF_4]$ (**4**) and $[(bpy)Pt(L'_{Ru})][BF_4]_2$ (**5**) showed similar features to those observed for **2** and **3** in terms of coordination and the square-planar geometry displayed by the platinum centers in both compounds. However, the Pt(bpy) unit remains planar with respect to the catecholate unit (hinge angle θ = 1°; 2°). Furthermore, unlike **2** and **3**, the solid-state packing of **4** and **5** revealed the presence of Pt···Pt interactions between individual units to form a dimer, which further undergoes a π−π interaction between another dimer to give a supramolecular one-dimensional (1D) chain (see Figure 2). This difference in structures is no doubt related to the organometallic quinonoid ligand, which might alter the electronic properties of the Pt(bpy) chromophore and promote these metal···metal interactions observed in complexes **4** and **5**.

Photophysics. The absorption spectra of the binuclear complexes, recorded in dilute CH_3CN solution ($c = 2 \times 10^{-5}$ M) at room temperature (rt), are reported in Figure 3, and relevant data are collected in Table 2. The prototype neutral complex **1**, without the Cp*M fragment coordinated to the quinone moiety, displays four bands in the high-energy region of the spectrum below 360 nm (Figure 3, Table 2). The bands at 290 and 360 nm have been assigned to charge-transfer transitions from the d orbital of the metal to π-antibonding orbitals of the α-diimine, while the bands at 245 and 320 nm have been assigned to intraligand π−π* transitions centered on the α-diimine fragment.[18] The above complex shows an additional band with a moderate extinction coefficient in the visible region of the spectrum, λ_{max} = 530 nm (ε_{max} = 5200 M^{-1}·cm^{-1}). This has been attributed to a charge-transfer transition involving the highest occupied molecular orbital (HOMO) mainly of dioxolenes and the lowest unoccupied molecular orbital (LUMO) exclusively of α-diimine.[18]

The singly charged complex **4** displays a similar envelope of absorption bands below 320 nm with respect to **1**. In the case of **4**, the lowest energy transition (λ_{max} = 525 nm) appears at ca. the same energy as in **1**, but with a greatly reduced intensity.

dx.doi.org/10.1021/ic500232w | Inorg. Chem. 2014, 53, 6624−6633

Table 1. Crystallographic Data and Structure Refinement Parameters for Compounds 2−5

	2·CH_3CN	**3**·CH_3CN	**4**·0.5CH_3CN·H_2O	**5**·CH_3CN
empirical formula	$C_{28}H_{30}B_2F_8N_3O_2PtRh$	$C_{28}H_{30}B_2F_8IrN_3O_2Pt$	$C_{27}H_{30.5}BF_4N_{2.5}O_3PtRu$	$C_{24}H_{21}B_2F_8N_3O_2PtRu$
formula weight (g/mol)	912.17	1001.46	821.01	853.22
temperature (K)	200(2)	200(2)	200(2)	200(2)
wavelength (Å)	0.710 73	0.710 73	0.710 73	0.710 73
crystal system	monoclinic	monoclinic	triclinic	monoclinic
space group	$P2_1/n$	$P2_1/n$	$P\bar{1}$	$P2_1/c$
unit cell dimensions	a = 11.3271(11) Å	a = 11.3386(10) Å	a = 10.5774(2) Å	a = 20.0763(13) Å
	b = 14.7963(12) Å	b = 14.8046(9) Å	b = 11.8718(2) Å	b = 14.2082(13) Å
	c = 18.2899(16) Å	c = 18.2950(14) Å	c = 13.9090(4) Å	c = 18.783(3) Å
	α = 90°	α = 90°	α = 107.132(1)°	α = 90°
	β = 91.149(8)°	β = 91.291(6)°	β = 95.780(1)°	β = 98.568(7)°
	γ = 90°	γ = 90°	γ = 114.127(1)°	γ = 90°
volume (Å^3)	3064.8(5)	3070.3(4)	1473.51(6)	5297.9(11)
Z	4	4	2	8
density calculated (Mg/m^3)	1.977	2.167	1.850	2.139
absorption coefficient (mm^{-1})	5.179	8.962	5.311	5.931
F(000)	1760	1888	794	3248
reflections collected	34 821	34 568	36 752	72 413
independent reflections	8896	8884	10 219	13 978
	R(int) = 0.0450	R(int) = 0.0485	R(int) = 0.0220	R(int) = 0.0509
final R indices [$I > 2\sigma(I)$]	$R1$ = 0.0325	$R1$ = 0.0315	$R1$ = 0.0284	$R1$ = 0.0580
	$wR2$ = 0.0756	$wR2$ = 0.0591	$wR2$ = 0.0684	$wR2$ = 0.011 41
R indices (all data)	$R1$ = 0.0509	$R1$ = 0.0624	$R1$ = 0.0402	$R1$ = 0.0962
	$wR2$ = 0.0842	$wR2$ = 0.0661	$wR2$ = 0.0744	$wR2$ = 0.1263
goodness-of-fit on F^2	1.004	1.006	1.042	1.059
largest diff. peak and hole (e Å^{-3})	1.056 and −2.078	1.053 and −1.050	1.833 and −0.982	3.898 and −2.681
CCDC number	974 242	974 243	974 244	974 245

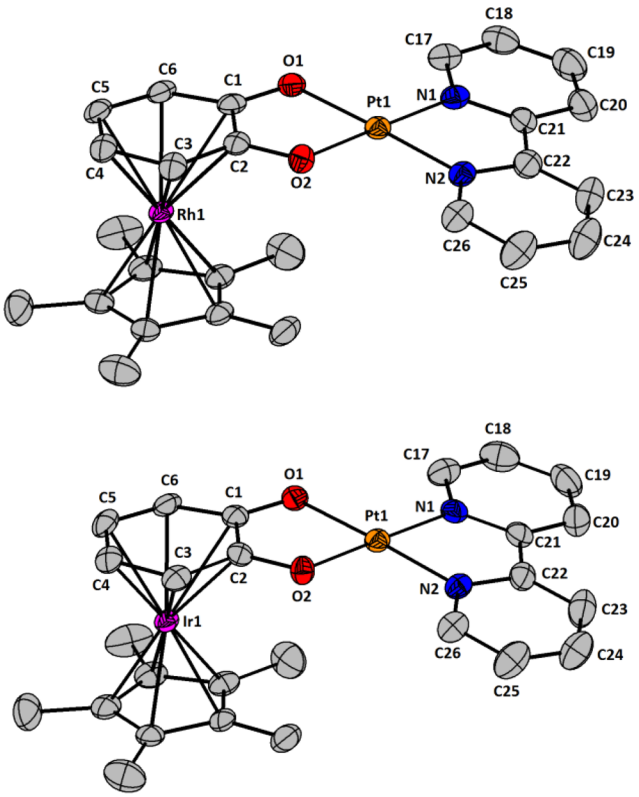

Figure 1. Molecular structures of complexes **2** (top) and **3** (bottom) with atom numbering system. Perspective views show thermal ellipsoids at 50% probability.

The Cp*Ru derivative **4** also shows the presence of a new band in the visible region with moderate extinction coefficient, which position is dependent on solvent poarity, that can be attributed to a mixed-metal-ligand-to-ligand charge transfer (CT) process.[19]

The doubly charged complexes **2**, **3**, and **5** display a very similar behavior, with the main differences located in the intensity of the high-energy band at 260 nm and in the position of the high-intensity band in the visible region at 390, 373, and 379 nm for the Rh, Ir, and Ru derivatives, respectively (Figure 3, Table 2).

Overall, for complexes **2**−**5**, the attribution to orbital transition of the observed absorption band is not straigthforward. In fact, the usual assumption used to interpret the spectroscopic properties of inorganic complexes, that both the ground and excited states can be described by a localized molecular orbital (MO) configuration, is less applicable in organometallic compounds, where a large degree of covalency in the metal−ligand bonds exists. For this, we applied DFT and TD-DFT methods to complexes **1**−**5**, and the results will be discussed in the following sections (vide infra).

All examined complexes are nonluminescent in deaerated solutions at rt, with the notable exception of **4**. At odds with this, all the complexes **1**−**5** were found to emit in glassy solution at 77 K. The luminescence spectra obtained at 77 K in MeOH/EtOH (1:4) mixture are reported in Figure 4, together with the emission spectrum of **4** in CH_2Cl_2 solution, while the relevant photophysical parameters are summarized in Table 2.

The mono cationic complex **4** shows a weak rt orange-red emission from CH_2Cl_2 solution (λ_{max} = 586 nm, ϕ = 3.4 × 10^{-3}, and τ = 56.4 ns), which increases upon removal of oxygen (ϕ = 4.1 × 10^{-3} and τ = 67.1 ns), as expected for excited-state

dx.doi.org/10.1021/ic500232w | Inorg. Chem. 2014, 53, 6624−6633

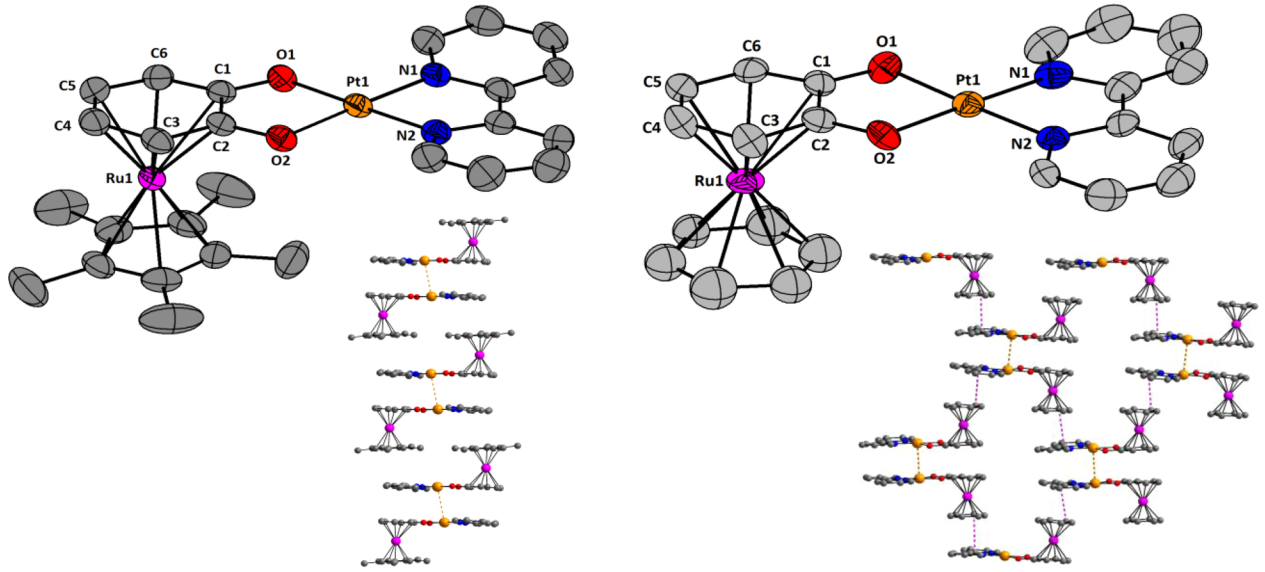

Figure 2. Molecular structures with atom numbering system and solid-state packing between individual units through Pt···Pt and $\pi-\pi$ interaction to generate a 1D supramolecular chain for **4** (left) and a two-dimensional network for **5** (right). Perspective views show thermal ellipsoids at 50% probability.

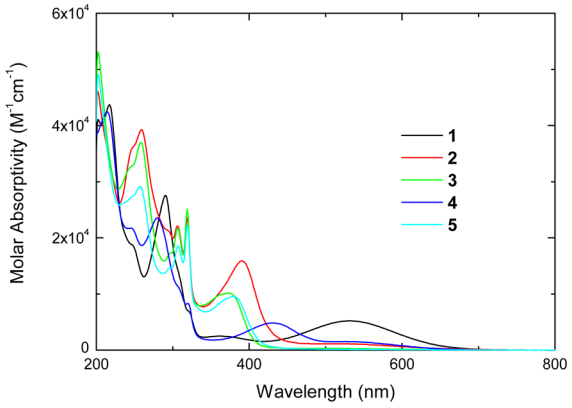

Figure 3. Absorption spectra of complexes **1**–**5** in CH_3CN solution at room temperature.

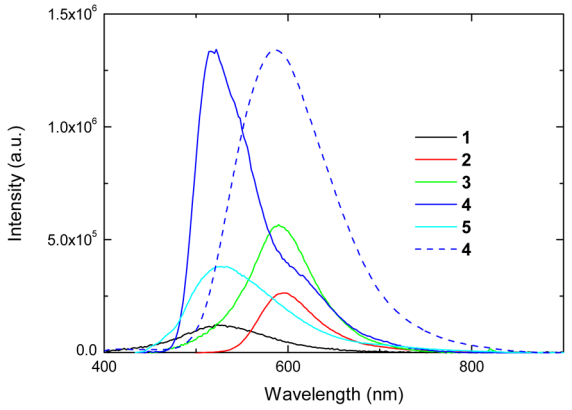

Figure 4. Emission spectra of **1**–**5** in MeOH/EtOH (1:4) solutions at 77 K (full lines) and of **4** in CH_2Cl_2 solution at rt (dotted line). A = 0.1 at λ_{ex} = 370 nm; the spectrum of **4** at rt has been normalized to that observed at rt.

Table 2. Photophysical Parameters for Complexes 1–5

	absorption[a]	emission[b]	
	λ_{max}, nm ($\varepsilon_{max} \times 10^{-3}$, $M^{-1}\cdot cm^{-1}$)	λ_{max}, nm	τ, μs
1	245sh (18.9), 290 (27.5), 320sh (7.0), 361 (2.5), 532 (5.2)	530	7.3
2	259 (39.3), 306 (22.1), 319 (23.6), 390 (15.9), 509 (1.1)	595 (601)	6.5
3	258 (37.0), 306 (21.7), 319 (25.1), 373 (10.1), 491 (0.3)	590 (553)	3.8
4	245 (21.7), 280 (23.6), 320 (8.3), 430 (4.8), 524 (1.5)	515 (514)	30.0
5	257 (29.1), 307 (18.5), 319 (22.2), 379 (9.5)	530 (516)	6.3

[a]In CH_3CN at rt; sh is shoulder. [b]In MeOH/EtOH (1:4) at 77 K; the calculated emission energies are reported in parentheses.

transitions originating from triplet states and involving singlet ground states. The experimental radiative rate constant, calculated as ϕ/τ, is $k_r = 6 \times 10^4$ s^{-1}, and it is comparable to that already observed for other organometallic Pt(II) square planar complexes with bpy ligands.[20] On switching from rt to 77 K, a large blue shift of the emission of ca. 2300 cm^{-1} is observed, while the shape of the spectrum remains rather broad. These results are consistent with a CT nature of the excited state. (On going from rt to 77 K, a hypsochromic shift of the emission is expected, since in the frozen state the reorganization of the solvent is prevented, and thus the CT state is destabilized.) The other ruthenium derivative, the dicationic complex **5**, shows at 77 K a weaker emission but with a similar energy with respect to **4**. In consideration of the similar nature of the luminescent excited state for **4** and **5**, the shorter lifetime observed in **5** is an indication of the lower emission quantum yield of the latter with respect to the Cp*Ru analogue.

The Rh and Ir derivatives display in glassy solution at 77 K an unstructured emission band, peaking around 590 nm with lifetimes in the μs range. The emission energy of complexes **2**–**5** can thus be tuned over a wide range from green to orange by coordinating the Cp*M, M = Rh, Ir, or Ru, or the (C_6H_6)Ru fragment onto the catecholate ligand. This has also the notable effect of increasing the luminescence intensity, especially when

dx.doi.org/10.1021/ic500232w | Inorg. Chem. 2014, 53, 6624–6633

Ru(II) is present. This effect has already been observed in a previous series of octahedral heteroleptic complexes with the same organometallic linker.[16]

DFT and TD-DFT Calculations. To elucidate the origin of the photophysical behavior of **1**−**5**, these complexes were investigated by means of DFT and TD-DFT methods.[21] A preliminary study of the calculated electron properties of **1** was performed to assess the validity of the adopted theoretical modeling for the investigated class of compounds by comparison with the experimental results herein presented, besides the available information in literature. The four high occupied and the four low virtual MOs of **1** are shown on the left-hand side of Figure 5. They evidence that the cathecolate

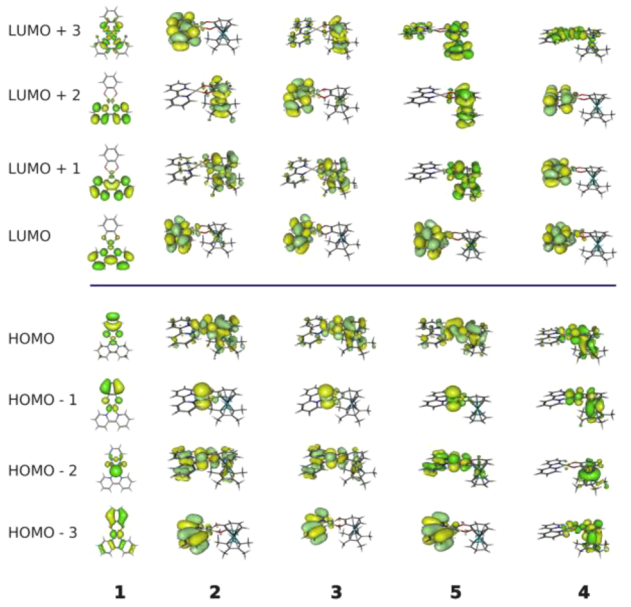

Figure 5. Calculated MOs of **1**−**5**.

(cat) ligand characterizes the high occupied MOs (HOMO and HOMO−1), while the bipyridine (bpy) ligand occupies the low virtual ones (LUMO, LUMO+1, and LUMO+2), in agreement with what was established by previous investigation on this class of complexes.[8,13] A significant contribution by the d orbitals of Pt(II) only occurs in the inner occupied MOs where the d_{z^2} orbital describes the HOMO−2, and in high virtual MOs where its $d\sigma^*$ orbital characterizes the LUMO+3. The charge distribution among cat, bpy, and Pt(II), obtained as a sum of natural charges calculated by means of the natural bond order (NBO) analysis[22] (Table 3) evidences that the electron density is polarized toward the cat unit. Moreover, the formally dicationic Pt compensates its lack of electrons through its

Table 3. Comparison among the NBO Partial Charges Summed over 1 with Those Summed over the Fragments

	1	cat[a]	bpy	Pt(II)	M[b]	Cp*/bz
1	0.00	−1.14 (−1.43)	+0.45	+0.70		
2	+1.11	−0.22 (−1.28)	+0.64	+0.69	+0.24	+0.65
3	+1.15	−0.17 (−1.27)	+0.64	+0.69	+0.08	+0.76
5	+1.27	−0.06 (−1.27)	+0.64	+0.69	−0.12	+0.86
4	+0.76	−0.46 (−1.35)	+0.57	+0.65	−0.14	+0.38

[a]The total partial charge of the oxygens is reported within brackets. [b]M = Rh(III), Ir(III), and Ru(II); Cp* = $C_5(CH_3)^-$; bz = C_6H_6

bonds with the two ligands. Actually, Pt acts both as an electron donor toward the Rydberg orbitals of the two ligands and as an electron acceptor from the occupied orbitals of the N and O atoms through its 5d6s atomic orbitals.

The MOs of the dicationic complexes **2**, **3**, and **5** show a very similar pattern among them (Figure 5). The comparison with those of **1** evidence that the formation of the L_M fragment (L_M = (cat)M(Cp*) or (cat)M(bz), M = Rh, Ir, or Ru; bz = benzene) largely stabilizes the energy of those MOs where the electron density is delocalized on cat, with respect to what was calculated for **1** itself. In fact, apart from the HOMOs, which correlate with that of **1**, the energy of the other occupied MOs delocalized on the L_M moiety containing the cat moiety is lower than that of those characterized by the d_{z^2} orbital of Pt or bpy. The same effect is observed in the virtual MOs, since those characterized by L_M occur at lower energy than those delocalized on bpy, besides the LUMO, which preserves the same characteristics of **1**. On the contrary, the low virtual orbitals of the monocation **4** (Figure 5) closely resemble those of **1**, with the electron density always delocalized on bpy up to LUMO+2. The comparison of the high occupied MOs of **4** with those of the dicationic complexes evidence that the electron density is largely delocalized on L_M in the monocation, besides the more important role played in their description by the d atomic orbitals of Ru. This aspect is particularly evident in HOMO−2, which is completely characterized by the d_{z^2} orbital of Ru, instead of by that of Pt.

Considering how the charge distribution of **1** is modified in the sandwich complexes (Table 3), one notes that the extra electron charge of cat is largely drained by the (Cp*/bz)M moiety to compensate the formally positive charges of the transition metals. On the whole, in the dicationic L_M complexes more than one electron charge is taken mainly from the aryl of **1** by the (Cp*/bz)M moiety, that is, 1.11 δ^+ (**2**), 1.15 δ^+ (**3**), and 1.27 δ^+ (**5**). In all cases partial positive charges of 0.67−0.68 δ^+ and 0.64 δ^+ are located at L_M (M + Cp*/bz + cat) and bpy, respectively, while that of Pt remains practically unchanged with respect to **1**, that is, 0.69 δ^+ versus 0.70 δ^+ in **1**. Nevertheless, the three dicationic complexes differentiate for the charge distribution within L_M since the ability of the (Cp*/bz)M moieties to attract electrons from cat increases in the following order **5** > **3** > **2**. Also in the case of the monocation **4** the **1** moiety (0.76 δ^+) acts as an electron donor toward the (Cp*)Ru unit, though a larger amount of the electron charge (0.46 δ^-) is left on cat. Substantially, Pt(II) always acts as a bridge for the exchange of electrons between the bpy and L_M ligands since its electronic partial charge within all complexes remains substantially unchanged. Altogether, the charge distribution analysis within the complexes and the characterization of the HOMO and LUMO suggest the rationale of the larger bandgap observed in **2**−**5** with respect to **1**, as indicated by the absorption spectra (vide infra). On the whole, the insertion of (Cp*/bz)M in **1** largely stabilizes the electronic energy of L_M.

To investigate the nature of phosphorescent emission at low temperature, **2**−**5** were modeled in vacuo neglecting the contribution by the methyl substituents of Cp* in the case of **2**−**4**. The structural relaxation in the lowest triplet state of the sandwich complexes (Supporting Information, Figure S1) is driven by the vibrational butterfly mode of **1**, and a large increase of the dihedral angle formed by the aryl and the (bpy) Pt plane by about 13° (**2**) and 24° (**3**) is calculated, while it only amounts to less than 4° in the Ru complexes. In fact, the

dx.doi.org/10.1021/ic500232w | Inorg. Chem. 2014, 53, 6624−6633

less positively charged Ru(II) atom (see Table 3) in **4** and **5** allows less flexibility to the structure of L_M during relaxation in the triplet state. An examination of NBOs of L_M shows that Ru evenly bonds to the C atoms only by means of its d orbitals. On the contrary, also spd hybrid orbitals of Rh and Ir preferentially bond selected C atoms, besides pure d orbitals. In the triplet state the unpaired electrons are largely delocalized at L_M in the dication sandwich complexes, while in the case of the monocation the bpy moiety is preferred (see Supporting Information, Figure S2). The trend shown by the T_1-S_0 energy gap, calculated by the ΔSCF method and reported in Table 2, is in fairly good agreement with that of the emission wavelengths, supporting the information gained by the simplified molecular modeling.

TD-DFT Calculations of the Excitation Spectra. The comparison among the absorption spectra of **1**−**5** recorded in CH_3CN solution (Figure 3) evidenced how the electronic structure of complexes **2**−**4** is largely influenced by their total charge. To gain a deeper insight into the origin of such behavior the electronic transitions of these complexes were investigated by means of TD-DFT focusing on the changes produced into the parent complex **1** by the formation of L_M. Moreover, the comparison among the absorption spectra of **2**−**5** with that of **1** evidence, in the case of **2** and **4**, a marked weakening of the observed intensity in the spectral region of the first absorption band of **1**. This can be attributed to the presence of triplet−triplet transitions, particularly in the case of **2**. In fact, the $S_0 \rightarrow S_1$ transitions of **2** and **4** are calculated at 379 and 448 nm, respectively.

The calculated absorption spectra are drawn in Figure 6 (**1** and **4**) and Figure 7 (**2**, **3**, and **5**) where the calculated

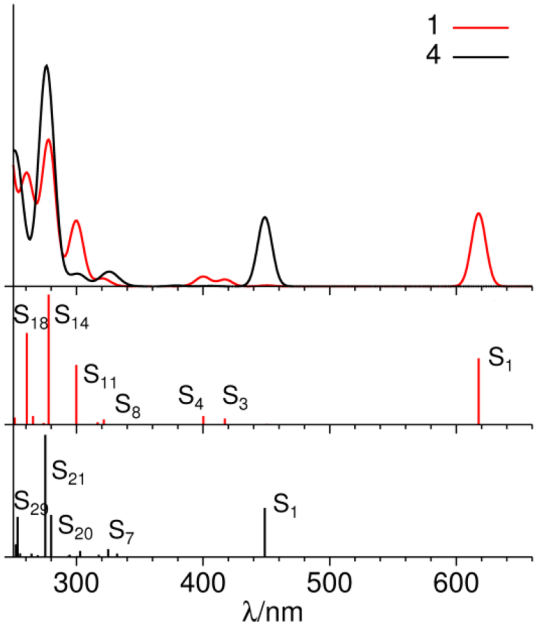

Figure 6. Simulated absorption spectra (upper) and calculated oscillator strengths (lower) for complexes **1** and **4**.

transitions (see Supporting Information, Table S2−S6) are also reported. In the case of **1** the first absorption band above 450 nm was already thoroughly investigated and assigned to $L_{cat}L_{bpy}$CT transitions.[8,13a] This absorption is mainly originated by the $S_0 \rightarrow S_1$ transition calculated at 617 nm with a significant intensity and the transition dipole moment oriented along the

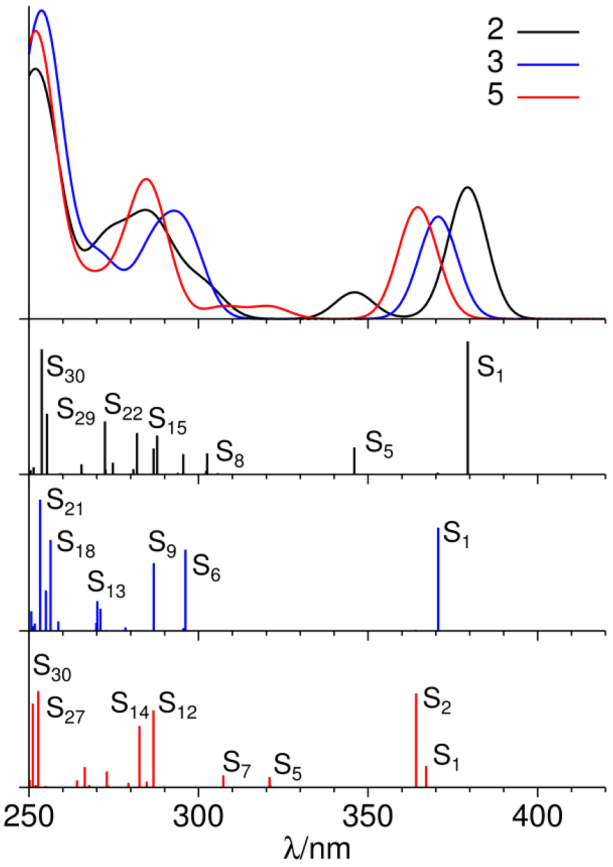

Figure 7. Simulated absorption spectra (upper) and calculated oscillator strengths (lower) for complexes **2**, **3**, and **5**.

long molecular axis. Also the weaker $S_0 \rightarrow S_2$ transition calculated at 450 nm owns the same $L_{cat}L_{bpy}$CT character, but its transition dipole moment is oriented along the short molecular axis. The wide broadening of this band was ascribed to the presence of singlet−triplet transitions, which occur in this range of wavelength and can be of considerable intensity due to the presence of the heavy atom effect induced by the Pt(II) center,[8] along with the vibronic broadening. At lower wavelengths another two $L_{cat}L_{bpy}$CT transitions ($S_0 \rightarrow S_3$ at 419 nm and $S_0 \rightarrow S_4$ at 403 nm) of weaker intensity occur both starting from the HOMO and ending up to LUMO+1 and LUMO+2, respectively. They contribute to the weak absorption band detected in the range of 340−420 nm, besides the $S_0 \rightarrow S_5$ transition (391 nm) with low intensity. This last involves excitations starting from the d_{z^2} orbital of Pt up to bpy (HOMO−2 to LUMO) and is the lowest energy transition with an $M_{Pt}L_{bpy}$CT character. The intense absorption band observed within the range of 260−330 nm is assigned to transitions $S_0 \rightarrow S_{8-18}$, having a mixed $L_{cat}L_{bpy}$CT and $M_{Pt}L_{bpy}$CT character. The $S_0 \rightarrow S_8$ transition calculated at 321 nm, in very good agreement with the experimental absorption, and the $S_0 \rightarrow S_{11}$ transition at 299 nm are characterized by $L_{cat}L_{bpy}$CT excitations. At lower wavelength also ligand centered (LC) excitations acquire relevance in the description of this absorption band, such as the intense transitions $S_0 \rightarrow S_{14}$ at 277 nm ($L_{bpy}C$) and $S_0 \rightarrow S_{18}$ at 260 nm ($L_{cat}C$). The remaining 24 transitions calculated from 200 to 251 nm give rise to the intense band at high energy. The most intense $S_0 \rightarrow S_{22}$ transition is calculated at 243 nm, in good agreement with the observed absorption at about 248 nm.

dx.doi.org/10.1021/ic500232w | Inorg. Chem. 2014, 53, 6624−6633

Transitions to higher singlet excited states are originated by multiple excitations.

Analogously to what discussed for **1**, the first absorption band of **4** is completely characterized by $L_{Ru}L_{bpy}CT$ excitations, which give rise to the intense $S_0 \rightarrow S_1$ (448 nm) and the weaker $S_0 \rightarrow S_2$ (405 nm) transitions. The $M_{Pt}L_{bpy}CT$ transitions occur at higher energy with respect to **1**, with $S_0 \rightarrow S_3$ (379 nm) and $S_0 \rightarrow S_4$ (341 nm) largely characterized by an excitation starting from the d_{z^2} orbital of Pt and of Ru, respectively, up to the bipyridyl moiety. The weak absorptions, down to 330 nm, contribute transitions up to $S_0 \rightarrow S_6$ having a mixed $L_{cat}L_{bpy}CT$ and $M_{Pt}L_{bpy}CT$ character. Similarly to **1**, the absorption at 320 nm is due to an $L_{Ru}L_{bpy}CT$ transition, namely, the $S_0 \rightarrow S_7$ transition calculated at 325 nm. To the intense band at lower wavelengths with a maximum at 285 nm, the $S_0 \rightarrow S_{8-26}$ transitions contribute. The strong intensity is mainly attributed to the transitions $S_0 \rightarrow S_{20}$ (279 nm) and $S_0 \rightarrow S_{21}$ (275 nm). This last very strong transition is largely due to an $L_{bpy}C$ excitation. Within the narrow range of 248−253 nm the fairly intense $S_0 \rightarrow S_{28-32}$ transitions are calculated, which mix $L_{Ru}C$ with $L_{Ru}L_{bpy}CT$ transitions. This kind of LC excitation also largely contributes to the description of the $S_0 \rightarrow S_{37-39}$ transitions calculated in the range of 238−240 nm.

In the case of the dication sandwich complexes **2**, **3**, and **5**, the first absorption bands in the range of 340−420 nm result farther blue-shifted and more intense with respect to those of the other two examined complexes. In agreement with the experimental findings, the $S_0 \rightarrow S_1$ transitions of **3** (370 nm) and **5** (367 nm) are calculated at lower wavelengths and with minor intensity than that of **2** (379 nm). Only in the case of **3** this transition preserves the pure $L_{Ir}L_{bpy}CT$ character as in **4**, while $L_{Rh}C$ excitations already contribute to this transition in **2**, and completely characterize its $S_0 \rightarrow S_2$ (370 nm) of weaker intensity. On the contrary, in the case of **5**, the $S_0 \rightarrow S_1$ and $S_0 \rightarrow S_2$ transitions, which are calculated very close in energy (ΔE = 0.02 eV), already mix the contribution by the HOMO−LUMO ($L_{Ru}L_{bpy}CT$) excitation with that arising from the d_{z^2} orbital of Pt (HOMO−1) up to the bipyridyl unit ($M_{Pt}L_{bpy}CT$). This last excitation largely characterizes the $S_0 \rightarrow S_1$ transition of minor calculated intensity than $S_0 \rightarrow S_2$ (364 nm) of **5**, besides the $S_0 \rightarrow S_3$ (363 nm) of **2** and the $S_0 \rightarrow S_2$ (364 nm) of **3**.

The two peaks recorded in the absorption spectra of all the dicationic complexes at about 319 and 307 nm are assigned to the $S_0 \rightarrow S_5$ and $S_0 \rightarrow S_7$ transitions in the case of **5**. They are calculated at 320 and 307 nm, respectively, in excellent agreement with the experimental peaks. They are both originated by a mixing of $L_{Ru}C$ and $ML_{Ru}CT$ excitations. The $S_0 \rightarrow S_5$ (345 nm) and $S_0 \rightarrow S_8$ (302 nm) of **2** are assigned to the above-mentioned observed peaks, since they are originated by an $L_{Rh}C$ excitation with significant intensity. Unfortunately, in the case of **3** these two peaks are poorly described by the present calculations, since an $L_{Ir}C$ excitation only occurs in $S_0 \rightarrow S_6$ calculated at 296 nm as a very intense transition.

At 295 nm a fairly intense absorption is calculated for the $S_0 \rightarrow S_{11}$ transition of **2**, in excellent agreement with the experimental data. It is attributed to $L_{Rh}C$ excitations starting from inner occupied MOs. Its assignment corresponds to that of the $S_0 \rightarrow S_{11}$ of **5** calculated at 298 nm as a weaker absorption. The (HOMO−3)−LUMO excitation, describing the lowest energy $L_{bpy}C$ excitation, characterizes the transitions of all three dicationic complexes: the $S_0 \rightarrow S_{15}$ of **2**, the $S_0 \rightarrow S_9$ of **3**, and the $S_0 \rightarrow S_{12}$ of **5**, which are calculated at 286 nm in all cases. The remaining calculated transitions up to $S_0 \rightarrow S_{42}$ originate the intense absorption bands with maxima at about 258 nm and shoulders at about 246 nm. In the case of **5**, the most intense transitions are the $S_0 \rightarrow S_{27}$, $S_0 \rightarrow S_{28}$, and $S_0 \rightarrow S_{30}$, all calculated within 251−252 nm, besides the intense $S_0 \rightarrow S_{32}$ calculated at 243 nm, which contributes to the shoulder. They collect together $L_{Ru}C$ and $L_{bpy}C$, along with excitations starting from Ru and Pt. In the case of **2** they correspond to the $S_0 \rightarrow S_{29}$ (255 nm), and the $S_0 \rightarrow S_{30}$ (253 nm) transitions, besides $S_0 \rightarrow S_{34}$ (246 nm), while in **3** they contribute to the $S_0 \rightarrow S_{19-21}$ (253−256 nm) and $S_0 \rightarrow S_{26}$ (246 nm) transitions.

CONCLUDING REMARKS

Here, we presented a combined experimental and theoretical study of a new series of supramolecular assemblies of (bpy)Pt(II) linked to an organometallic ligand (cat)M(Cp*/bz). These have been synthesized and fully characterized, and for four complexes **2**−**5** the XRD molecular structures are reported. The photophysical properties of all complexes **1**−**5** were studied in solution at rt and in condensed media at low temperature.

All supramolecular assemblies **2**−**5** displayed a bright emission at low temperature, in contrast to the parent (bpy)Pt(cat) (**1**), highlighting the positive role of the coordination of the M(Cp*/bz) fragment to the cat ligand in turning on the luminescence properties. Notably, the Ru(Cp*) derivative (**4**) showed phosphorescence already in solution at rt with moderate quantum yield.

The electronic properties of **2**−**5** were examined by means of DFT and TD-DFT methods focusing on the modifications induced on the parent complex **1** after the formation of the organometallic ligand L_M. The good agreement obtained among the observed and calculated absorption spectra allows us to confidently discuss the different role played by the monocation $[Ru(Cp^*)]^{1+}$ and the dications $[M(Cp^*)]^{2+}$ (M = Rh, and Ir) and $[Ru(bz)]^{2+}$ in modulating the electronic states of this class of complexes with respect to **1** alone. The HOMO−LUMO gap increases with the oxidation number, due to the stabilization of the energy of those MOs characterized by the cat ligand, which significantly contributes to the description of the HOMO in all cases. Moreover, the deep reorganization of the MOs in the dication complexes makes the d_{z^2} orbital of Pt available for transitions to low excited states. The natural bond population (NBO)[22] analysis shows that Pt always acts as a bridge between the two ligands and favors the flow of electron density from the bpy toward the cat ligand to the metal atom in L_M. A high-amplitude wagging vibrational mode in a butterfly fashion of the (bpy)Pt(cat) fragment drives the relaxation of the complexes in the triplet state where the structures of **2** and **3** result largely distorted with respect to the two planes. On the contrary, sandwich complexes with Ru show fewer attitudes to undergo this kind of deformation. In fact, Ru evenly bonds to the C atoms within L_M by means of only its d atomic orbitals, while the spd hybrid orbitals of Rh and Ir contribute to the formation of preferential bonds with selected C atoms within L_M.

EXPERIMENTAL SECTION

All experimental manipulations were carried out under argon using Schlenk tube techniques. All solvents were purified and dried by standard techniques. The ^1H NMR and ^{13}C NMR spectra were recorded using a Bruker Avance 300 NMR spectrometer. Infrared spectra were recorded from neat samples on a Bruker FT-IR

dx.doi.org/10.1021/ic500232w | Inorg. Chem. 2014, 53, 6624−6633

spectrometer Tensor 27 equipped with an ATR Harricks. Elemental analyses were performed by microanalytical service of ICSN at Gif-sur-Yvette on a PerkinElmer 2400 apparatus.

Synthesis of [(bpy)Pt(cat)] (1). This compound was prepared following a modified procedure to that reported in the literature[17] and was obtained in higher yield. A Schlenk tube containing a mixture of [(bpy)$PtCl_2$] (420 mg, 1.0 mmol), catechol (120 mg, 1.1 mmol), and Cs_2CO_3 (717 mg, 2.2 mmol) in methanol (20 mL) and dimethylsulfoxide (2 mL) was allowed to reflux for 6 h. Then methanol was removed under reduced pressure, and water (50 mL) was added to the dark violet residue. The resulting precipitate was separated and washed with two more portions of water (20 mL each) and dried under vacuum; subsequent dissolution in dichloromethane (300 mL) and filtration through Celite provided a violet filtrate that, upon solvent evaporation, gave the desired compound [(bpy)Pt(cat)] (**1**) (315 mg, 0.69 mmol). Yield: 69%. Anal. Calcd for $C_{16}H_{12}N_2O_2Pt\cdot 0.5H_2O$ (468.4 g·mol^{-1}): C, 41.03; H, 2.80; N, 5.98. Found: C, 41.45; H, 2.68; N, 5.46%. ^{1}H NMR (300.13 MHz, CD_2Cl_2) δ 9.35 (d, 2H, ^3J = 6.0 Hz, H_6), 8.13 (m, 2H, H_4) 7.93 (d, 2H, ^3J = 9.0 Hz, H_3), 7.56 (m, 2H, H_5), 6.66 (dd, ^3J = 6.0 Hz, ^4J = 3.0 Hz, 2H, $C_6H_4O_2$), 6.38 (dd, ^3J = 6.0 Hz, ^4J = 3.0 Hz, 2H, $C_6H_4O_2$), ^{13}C(-^{1}H) NMR (75.45 MHz, CD_2Cl_2) δ 115.4 (C═C, $C_6H_4O_2$), 117.5 (C═C, $C_6H_4O_2$), 123.6 (bpy), 128.1 (bpy), 138.9 (bpy), 150.5 (bpy), 157.1 (bpy) 164.2 (C−O, $C_6H_4O_2$).

Synthesis of [(bpy)Pt(L_{Rh})][BF_4]$_2$ (2). To a red suspension of [Cp^*RhCl_2]$_2$ (163 mg, 0.21 mmol) in acetone (10 mL) was added a solution of $AgBF_4$ (160 mg, 0.82 mmol) in acetone (10 mL), and the mixture was stirred for 20 min at rt. Then the mixture was filtered through cotton into a Schlenk tube containing [(bpy)Pt(cat)] (195 mg, 0.43 mmol) in acetone (5 mL), and the mixture was stirred overnight at rt. Then the solvent was removed under reduced pressure, and the residue was washed with two portions of dichloromethane (15 mL each) and dried under vacuum. The green-yellowish microcrystalline solid was identified as [(bpy)Pt(L_{Rh})][BF_4]$_2$ (**2**) (321 mg; 0.37 mmol). Yield: 88%. Anal. Calcd for $C_{26}H_{27}B_2F_8N_2O_2RhPt$ (871.1 g·mol^{-1}): C, 35.85; H, 3.12; N, 3.22. Found: C, 35.98; H, 3.04; N, 3.04%. ^{1}H NMR (300.13 MHz, CD_3CN) δ 8.78 (d, 2H, ^3J = 5.4 Hz, $^3J_{H-Pt} \approx$ 40 Hz, H_6), 8.36 (ddd, 2H, ^3J = 8.1 Hz, $^3J_{H-H}$ = 8.3 Hz, $^4J_{H-H}$ = 1.6 Hz, H_4), 8.28 (d, 2H, ^3J = 8.1 Hz, H_3), 7.75 (ddd, 2H, ^3J = 8.1 Hz, $^3J_{H-H}$ = 8.3 Hz, $^4J_{H-H}$ = 1.3 Hz, H_5), 6.27 (m, 4H, H_α, H_β $C_6H_4O_2$), 2.07 (s, 15H, Cp*). ^{13}C(-^{1}H) NMR (75.45 MHz, CD_3CN) δ 9.8 (CH_3, Cp*), 93.2 (d, $^1J_{Rh-C}$ = 5.4 Hz, C═C, $C_6H_4O_2$), 95.2 (d, $^1J_{Rh-C}$ = 6.4 Hz, C═C, $C_6H_4O_2$), 107.4 (d, $^1J_{Rh-C}$ = 7.8 Hz, C═C, Cp*), 125.2 (bpy, C_3), 129.2 (bpy, C_5), 142.5 (bpy, C_4), 150.7 (bpy, C_6), 154.6 (bpy, C_2), 157.6 ((bpy, C_4). IR (neat ATR Harricks, cm^{-1}): ν(BF_4^-) 1025; ν(C═O) 1613.

Synthesis of [(bpy)Pt(L_{Ir})][BF_4]$_2$ (3). This compound was prepared following the procedure described for **2** except for the use of [Cp^*IrCl_2]$_2$ (120 mg, 0.15 mmol) instead of [Cp^*RhCl_2]$_2$ and $AgBF_4$ (116 mg, 0.60 mmol). The resulting solvated Cp*Ir moiety was added to a Schlenk tube containing [(bpy)Pt(cat)] (140 mg, 0.30 mmol), and subsequent treatment afforded the greyish microcrystalline solid that was identified as [(bpy)Pt(L_{Ir})][BF_4]$_2$ (**3**) (230 mg; 0.24 mmol). Yield: 80%. Anal. Calcd for $C_{26}H_{27}B_2F_8N_2O_2IrPt.2H_2O$ (996.4 g·mol^{-1}): C, 31.34; H, 3.14; N, 2.81. Found: C, 31.31; H, 2.62; N, 2.85%. ^{1}H NMR (300.13 MHz, CD_3CN) δ 8.73 (d, 2H, ^3J = 5.3 Hz, $^3J_{H-Pt} \approx$ 40 Hz, H_6), 8.35 (ddd, 2H, ^3J = 8.1 Hz, $^3J_{H-H}$ = 8.3 Hz, $^4J_{H-H}$ = 1.6 Hz, H_4), 8.26 (d, 2H, ^3J = 8.1 Hz, H_3), 7.73 (ddd, 2H, ^3J = 8.1 Hz, $^3J_{H-H}$ = 8.3 Hz, $^4J_{H-H}$ = 1.3 Hz, H_5), 6.42 (dd, 2H, ^3J = 4.5 Hz, ^4J = 2.7 Hz, H_β $C_6H_4O_2$), 6.24 (dd, 2H, ^3J = 4.5 Hz, ^4J = 2.7 Hz, H_α $C_6H_4O_2$), 2.16 (s, 15H, Cp*). ^{13}C(-^{1}H) NMR (75.45 MHz, CD_3CN) δ 9.4 (CH_3, Cp*), 85.1 (C═C, $C_6H_4O_2$), 87.5 (C═C, $C_6H_4O_2$), 100.9 (C═C, Cp*), 125.2 (bpy, C_3), 129.2 (bpy, C_5), 142.5 (bpy, C_4), 150.7 (bpy, C_6), 151.6 (bpy, C_2), 157.6 ((bpy, C_4). IR (neat ATR Harricks, cm^{-1}): ν(BF_4^-) 1027; ν(C═O) 1615.

Synthesis of [(bpy)Pt(L_{Ru})][BF_4] (4). This compound was prepared following the procedure described for complex **2** except for the use of [$Cp^*Ru(CH_3CN)_3$][BF_4] (45 mg, 0.10 mmol) instead of [Cp^*RhCl_2]$_2$ and $AgBF_4$. The solvated ruthenium compound in acetone was added to a Schlenk tube containing [(bpy)Pt(cat)] (50 mg, 0.10 mmol), and subsequent treatment afforded an orange microcrystalline solid identified as [(bpy)Pt(L_{Ru})][BF_4] (**4**) (63 mg; 0.08 mmol). Yield: 80%. Anal. Calcd for $C_{26}H_{27}BF_4N_2O_2RuPt\cdot 0.5CH_3CN\cdot H_2O$ (821.0 g·mol^{-1}): C, 39.50; H, 3.74; N, 4.27. Found: C, 39.73; H, 3.63; N, 4.57%. ^{1}H NMR (300.13 MHz, CD_3CN) δ 8.95 (d, 2H, ^3J = 5.4 Hz, $^3J_{H-Pt} \approx$ 40 Hz, H_6), 8.32 (ddd, 2H, ^3J = 8.1 Hz, $^3J_{H-H}$ = 8.3 Hz, $^4J_{H-H}$ = 1.6 Hz, H_4), 8.23 (d, 2H, ^3J = 8.1 Hz, H_3), 7.70 (ddd, 2H, ^3J = 8.1 Hz, $^3J_{H-H}$ = 8.3 Hz, $^4J_{H-H}$ = 1.3 Hz, H_5), 5.35 (dd, 2H, ^3J = 4.5 Hz, ^4J = 2.7 Hz, H_β $C_6H_4O_2$), 4.95 (dd, 2H, ^3J = 4.5 Hz, ^4J = 2.7 Hz, H_α $C_6H_4O_2$), 1.91 (s, 15H, Cp*). ^{13}C(-^{1}H) NMR (75.45 MHz, CD_3CN) δ 10.2 (CH_3, Cp*), 81.3 (C═C, $C_6H_4O_2$), 92.5 (C═C, $C_6H_4O_2$) 124.8 (bpy, C_3), 128.9 (bpy, C_5), 139.6 (bpy, C_4), 141.0 (bpy, C_6), 150.0 (bpy, C_2), 157.6 ((bpy, C_4). IR (neat ATR Harricks, cm^{-1}): ν(BF_4^-) 1034; ν(C═O) 1610.

Synthesis of [(bpy)Pt(L'_{Ru})][BF_4]$_2$ (5). This compound was prepared following the procedure described for **2** except for the use of [$(C_6H_6)RuCl_2$]$_2$ (65 mg, 0.12 mmol) instead of [Cp^*RhCl_2]$_2$ and $AgBF_4$ (99 mg, 0.50 mmol). The resulting solvated Cp*Ru moiety was added to a Schlenk tube containing [(bpy)Pt(cat)] (115 mg, 0.25 mmol), and subsequent treatment afforded a greyish microcrystalline solid identified as [(bpy)Pt(L'_{Ru})][BF_4]$_2$ (**5**) (180 mg; 0.23 mmol). Yield: 92%. Anal. Calcd for $C_{22}H_{18}B_2F_8N_2O_2RuPt\cdot H_2O$ (830.1 g·mol^{-1}): C, 31.84; H, 2.43; N, 3.37. Found: C, 32.12; H, 2.19; N, 3.13%. ^{1}H NMR (300.13 MHz, CD_3CN) δ 8.69 (d, 2H, ^3J = 5.4 Hz, $^3J_{H-Pt} \approx$ 40 Hz, H_6), 8.32 (ddd, 2H, ^3J = 8.1 Hz, $^3J_{H-H}$ = 8.3 Hz, $^4J_{H-H}$ = 1.6 Hz, H_4), 8.23 (d, 2H, ^3J = 8.1 Hz, H_3), 7.74 (ddd, 2H, ^3J = 8.1 Hz, $^3J_{H-H}$ = 8.3 Hz, $^4J_{H-H}$ = 1.3 Hz, H_5), 6.46 (s, 6H, C_6H_6), 6.36 (dd, 2H, ^3J = 4.5 Hz, ^4J = 2.7 Hz, H_β $C_6H_4O_2$), 5.88 (dd, 2H, ^3J = 4.5 Hz, ^4J = 2.7 Hz, H_α $C_6H_4O_2$). ^{13}C(-^{1}H) NMR (75.45 MHz, CD_3CN) δ 82.8 (C═C, $C_6H_4O_2$), 86.2 (C═C, $C_6H_4O_2$), 92.7 (C═C, C_6H_6), 125.2 (bpy, C_3), 129.1 (bpy, C_5), 142.4 (bpy, C_4), 150.8 (bpy, C_6), 152.6 (bpy, C_2), 157.4 ((bpy, C_4). IR (neat ATR Harricks, cm^{-1}): ν(BF_4^-) 1029; ν(C═O) 1612.

X-ray Crystallography for 2, 3, 4, and 5. Convenient crystals for X-ray analysis were grown at rt by slow diffusion of diethyl ether into CH_3CN solutions of the compounds. A single crystal of each compound was selected, mounted onto a cryoloop, and transferred in a cold nitrogen gas stream. For **2**, **3**, and **5**, intensity data were collected with a Bruker-Nonius KappaCCD diffractometer. Unit-cell parameters determination, data collection strategy, and integration were carried out with the Nonius EVAL-14[23] suite of programs. For **4**, intensity data were collected with a Bruker Kappa-APEXII diffractometer. Data collection was performed with APEX2 suite (Bruker). Unit-cell parameters refinement, integration, and data reduction were carried out with SAINT program (Bruker). SADABS (Bruker) was used for scaling and multiscan absorption corrections. In the WinGX suite of programs,[24] the structures of **2** and **5** were solved with Sir92 program,[25] while the structures of **3** and **4** were solved with ShelXS.[26] All were refined by full-matrix least-squares methods using SHELXL-97. All non-hydrogen atoms of cations were refined anisotropically except the disordered atoms of benzene ring in **5**. In all crystal structures, one of the BF_4 anions is disordered and sometimes refined isotropically. Hydrogen atoms were placed at calculated positions. DIAMOND[27] was used to create graphical illustrations. Supplementary crystallographic data are available in the Supporting Information.

Computational Details. The calculations were performed within the framework of the DFT using the exchange-correlation functional PBE0[28] included in the GAUSSIAN 09[29] program package. The effective core potentials (ECPs) of the Stuttgart/Cologne group were employed to account for the inner-shell electrons of the transition metals. Particularly, the small-core relativistic energy-consistent pseudopotentials (PPs) were used, along with their correlation consistent basis sets of *triple-ξ* quality for the 4d Ru and Rh (ECP28MDF/VTZ basis set),[30] and the 5d for Pt and Ir (ECP60MDF/VTZ basis set)[31] transition metals. The peculiarity of these PPs is that they incorporate both scalar and spin−orbit relativistic effects and are expected to be definitely more appropriate to describe the transition metals, particularly when relativistic effects

dx.doi.org/10.1021/ic500232w | Inorg. Chem. 2014, 53, 6624−6633

are large. The 6-31G* basis set[32] was employed for all of the other atoms. The S_0 geometries of the complexes were optimized with the default thresholds using a very fine prune grid in all calculations (Int = UltraFineGrid in Gaussian 09) for numerical integration to reach the minimum on the very flat potential energy surfaces. The energy gradients were always converged down to 10^{-4} au with the energies always converged by less than 4×10^{-6} hartrees (1×10^{-4} eV). The singlet−singlet excited-state transitions of the sandwich complexes were calculated by the TD-DFT[21] also using the TD-PBE0 method. To assign the absorption spectra of the sandwich complexes 42 singlet−singlet transitions were calculated with wavelengths starting from about 230 up to 380 nm for the dication **2**, **3**, and **5**, and up to 450 nm for **4**, while only 20 transitions of **1** cover the range of wavelength 250−630 nm. The solvation effects were always accounted for by using the default integral equation formalism (IEFPCM) variant of the polarizable continuum model (PCM)[33] to compare the calculated with the experimental absorption spectra in acetonitrile solution. The electron distribution of the complexes was investigated by means of the natural bond orbital population analysis (NBO program version 3.1)[22a,c] to obtain the charge distribution within the complexes.

To investigate the nature of phosphorescent emission at low temperature, complexes **2**−**5** were modeled in vacuo neglecting the contribution by the methyl substituents of Cp*. The optimization of the geometries of the lowest triplet state (T_1) were carried out using the quadratically convergent SCF procedure (SCF = QC) to calculate the MOs from the default initial guess, besides the Int = UltraFineGrid option. The transition energies were calculated by the ΔSCF method at the minimum energies of the T_1 and S_0 electronic states. The stability of the optimized structures was always confirmed by the calculated harmonic frequencies (Supporting Information, Table S16), and the appropriateness of the unrestricted Kohn−Sham orbitals was verified since the calculated spin contamination of T_1 after the annihilation of the first contaminant was at most 4×10^{-4} in the case of **5**.

The simulations of the electronic spectra were obtained by summing up Gaussian functions centered at each calculated wavelength with the height of the maxima related to the oscillator strength with a full width at half-maximum (fwhm) of 60 nm. The electron density plots were drawn by the Gabedit[34] software using the 0.025 isovalue parameter for countouring.

Photophysics. Absorption spectra of dilute solutions ($c = 2 \times 10^{-5}$ M) of CH_3CN were obtained using PerkinElmer Lambda 950 UV/vis/NIR spectrophotometer. Steady-state photoluminescence spectra were measured in air-equilibrated and deaerated solutions at rt, using an Edinburgh FLS920 fluorimeter, equipped with a Peltier-cooled R928 (200−850 nm) Hamamatsu PMT at the excitation wavelength of λ_{ex} = 370 nm. Luminescence quantum yields (φ) at rt were evaluated by comparing wavelength integrated intensities (I) of the corrected emission spectra with reference $[Ru(bpy)_3]Cl_2$ (φ_r = 0.028 in air-equilibrated water),[35] by using the following equation:

$$\varphi = \varphi_r \frac{(In^2/A)}{(I_r n_r^2/A_r)}$$

where A and A_r are the absorbance values at the employed excitation wavelength, and n and n_r are the refractive indexes of the solvents, respectively, for the investigated and the reference compound. The concentration was adjusted to obtain absorbance values $A \leq 0.1$ at the excitation wavelengths. Band maxima and relative luminescence intensities are obtained with uncertainties of 2 nm and 10%, respectively.

Luminescence lifetimes were obtained using a Jobin-Yvon IBH 5000F TCSPC apparatus equipped with a TBX Picosecond Photon Detection Module and NanoLED pulsed excitation sources. Analysis of luminescence decay profiles against time was accomplished using the Decay Analysis Software DAS6 provided by the manufacturer. The lifetime values were obtained with an estimated uncertainty of 10%.

Luminescence measurements of CH_3OH/C_2H_5OH (1:4) frozen glassy solutions at 77 K were performed by employing quartz capillary tubes immersed in liquid nitrogen and hosted within homemade quartz coldfinger dewar. Luminescence lifetimes at 77 K were obtained using both SpectraLED and NanoLED excitation sources.

■ ASSOCIATED CONTENT

Supporting Information

Crystallographic data of **2**, **3**, **4**, and **5** (CIF) and additional computational data. This material is available free of charge via the Internet at http://pubs.acs.org. CCDC 974242−974245 contain the supplementary crystallographic data for this paper. The data can be obtained free of charge from The Cambridge Crystallographic Data Centre via www.ccdc.cam.ac.uk/data_request/cif.

■ AUTHOR INFORMATION

Corresponding Authors

*E-mail: hani.amouri@upmc.fr. (H.A.)
*E-mail: andrea.barbieri@isof.cnr.it. (A.B.)

Notes

The authors declare no competing financial interest.

■ ACKNOWLEDGMENTS

This work was supported by the Centre National de la Recherche Scientifique, by the Université Pierre et Marie Curie-Paris 6, by French Agence Nationale de la Recherche grant (Project OPTOELECTR-OM ANR-11-BS07-001-01), and by the Italian Consiglio Nazionale delle Ricerche (Project PM.P04.010 "Materiali Avanzati per la Conversione di Energia Luminosa", MACOL), which we gratefully acknowledge. A.B. also thanks Mr. G. Bragaglia (CNR-ISOF) for technical assistance in the interfacing of the instrumentation to personal computer.

■ REFERENCES

(1) Hissler, M.; McGarrah, J. E.; Connick, W. B.; Geiger, D. K.; Cummings, S. D.; Eisenberg, R. *Coord. Chem. Rev.* **2000**, *208*, 115−137.

(2) (a) Chan, S. C.; Chan, M. C. W.; Wang, Y.; Che, C. M.; Cheung, K. K.; Zhu, N. Y. *Chem.—Eur. J.* **2001**, *7*, 4180−4190. (b) Furuta, P. T.; Deng, L.; Garon, S.; Thompson, M. E.; Frechet, J. M. J. *J. Am. Chem. Soc.* **2004**, *126*, 15388−15389.

(3) Chang, C. C.; Pfennig, B.; Bocarsly, A. B. *Coord. Chem. Rev.* **2000**, *208*, 33−45.

(4) Du, P. W.; Knowles, K.; Eisenberg, R. *J. Am. Chem. Soc.* **2008**, *130*, 12576−12577.

(5) Botchway, S. W.; Charnley, M.; Haycock, J. W.; Parker, A. W.; Rochester, D. L.; Weinstein, J. A.; J. Williams, A. G. *Proc. Natl. Acad. Sci. U. S. A.* **2008**, *105*, 16071.

(6) (a) Connick, W. B.; Geiger, D.; Eisenberg, R. *Inorg. Chem.* **1999**, *38*, 3264−3265. (b) Tears, D. K. C.; McMillin, D. R. *Coord. Chem. Rev.* **2001**, *211*, 195−205.

(7) Chassot, L.; Von Zelewsky, A.; Sandrini, D.; Maestri, M.; Balzani, V. *J. Am. Chem. Soc.* **1986**, *108*, 6084−6085.

(8) Weinstein, J. A.; Tierney, M. T.; Davies, E. S.; Base, K.; Robeiro, A. A.; Grinstaff, M. W. *Inorg. Chem.* **2006**, *45*, 4544−4555.

(9) (a) Chan, C. W.; Cheng, L. K.; Che, C. M. *Coord. Chem. Rev.* **1994**, *132*, 87−97. (b) Hissler, M.; Connick, W. B.; Geiger, D. K.; McGarrah, J. E.; Lipa, D.; Lachicotte, R. J.; Eisenberg, R. *Inorg. Chem.* **2000**, *39*, 447−457. (c) Hua, F.; Kinayyigit, S.; Cable, J. R.; Castellano, F. N. *Inorg. Chem.* **2005**, *44*, 471−473. (d) Li, Y. G.; Tam, A. Y. Y.; Wong, K. M. C.; Li, W.; Wu, L. X.; Yam, V. W. W. *Chem.—Eur. J.* **2011**, *17*, 8048−8059. (e) Pomestchenko, I. E.; Luman, C. R.; Hissler, M.; Ziessel, R.; Castellano, F. N. *Inorg. Chem.* **2003**, *42*, 1394−1396. (f) Shavaleev, N. M.; Bell, Z. R.; Easun, T. L.; Rutkaite, R.; Swanson, L.; Ward, M. D. *Dalton Trans.* **2004**, 3678−3688. (g) Wadas, T. J.;

Chakraborty, S.; Lachicotte, R. J.; Wang, Q. M.; Eisenberg, R. *Inorg. Chem.* **2005**, *44*, 2628−2638. (h) Yam, V. W. W.; Tang, R. P. L.; Wong, K. M. C.; Cheung, K. K. *Organometallics* **2001**, *20*, 4476−4482.
(10) Wilson, M. H.; Ledwaba, L. P.; Field, J. S.; McMillin, D. R. *Dalton Trans.* **2005**, 2754−2759.
(11) (a) Boyer, J. L.; Rochford, J.; Tsai, M. K.; Muckerman, J. T.; Fujita, E. *Coord. Chem. Rev.* **2010**, *254*, 309−330. (b) Kaim, W.; Sarkar, B. *Coord. Chem. Rev.* **2007**, *251*, 584−594. (c) Meacham, A. P.; Druce, K. L.; Bell, Z. R.; Ward, M. D.; Keister, J. B.; Lever, A. B. P. *Inorg. Chem.* **2003**, *42*, 7887−7896. (d) Ward, M. D.; McCleverty, J. A. *J. Chem. Soc., Dalton Trans.* **2002**, 275−288.
(12) (a) Fox, G. A.; Pierpont, C. G. *Inorg. Chem.* **1992**, *31*, 3718−3723. (b) Kinder, J. D.; Youngs, W. J. *Organometallics* **1996**, *15*, 460−463. (c) Lesley, M. J. G.; Clegg, W.; Marder, T. B.; Norman, N. C.; Orpen, A. G.; Scott, A. J.; Starbuck, J. *Acta Crystallogr., Sect. C: Cryst. Struct. Commun.* **1999**, *55*, 1272−1275. (d) Sarkar, B.; Hubner, R.; Pattacini, R.; Hartenbach, I. *Dalton Trans.* **2009**, 4653−4655.
(13) (a) Best, J.; Sazanovich, I. V.; Adams, H.; Bennett, R. D.; Davies, E. S.; Meijer, A.; Towrie, M.; Tikhomirov, S. A.; Bouganov, O. V.; Ward, M. D.; Weinstein, J. A. *Inorg. Chem.* **2010**, *49*, 10041−10056. (b) Shavaleev, N. M.; Davies, E. S.; Adams, H.; Best, J.; Weinstein, J. A. *Inorg. Chem.* **2008**, *47*, 1532−1547.
(14) (a) Amouri, H. *Synlett* **2011**, 1357−1369. (b) Amouri, H.; Caspar, R.; Gruselle, M.; Guyard-Duhayon, C.; Boubekeur, K.; Lev, D. A.; Collins, L. S. B.; Grotjahn, D. B. *Organometallics* **2004**, *23*, 4338−4341. (c) Amouri, H.; Vaissermann, J.; Besace, Y.; Vollhardt, K. P. C.; Ball, G. E. *Organometallics* **1993**, *12*, 605−609. (d) Amouri, H.; Malezieux, B.; Thouvenot, R.; Vaissermann, J.; Gruselle, M. *Organometallics* **2001**, *20*, 1904−1906. (e) Vichard, D.; Gruselle, M.; Amouri, H. *J. Chem. Soc., Chem. Comm.* **1991**, 46−48. (f) Amouri, H.; Moussa, J.; Renfrew, A. K.; Dyson, P. J.; Rager, M. N.; Chamoreau, L. M. *Angew. Chem., Int. Ed.* **2010**, *49*, 7530−7533. (g) Amouri, H.; Thouvenot, R.; Gruselle, M. *C. R. Chim.* **2002**, *5*, 257−262. (h) Moussa, J.; Lev, D. A.; Boubekeur, K.; Rager, M. N.; Amouri, H. *Angew. Chem., Int. Ed.* **2006**, *45*, 3854−3858. (i) Moussa, J.; Rager, M. N.; Boubekeur, K.; Amouri, H. *Eur. J. Inorg. Chem.* **2007**, 2648−2653.
(15) (a) Moussa, J.; Amouri, H. *Angew. Chem., Int. Ed.* **2008**, *47*, 1372−1380. (b) Moussa, J.; Rager, M. N.; Chamoreau, L. M.; Ricard, L.; Amouri, H. *Organometallics* **2009**, *28*, 397−404. (c) Moussa, J.; Wong, K. M.-C.; Le Goff, X. F.; Rager, M. N.; Chan, C. K.-M.; Yam, V. W.-W.; Amouri, H. *Organometallics* **2013**, *32*, 4985−4992. (d) Moussa, J.; Wong, K. M. C.; Chamoreau, L. M.; Amouri, H.; Yam, V. W. W. *Dalton Trans.* **2007**, 3526−3530.
(16) (a) Damas, A.; Ventura, B.; Axet, M. R.; Degli Esposti, A.; Chamoreau, L. M.; Barbieri, A.; Amouri, H. *Inorg. Chem.* **2010**, *49*, 10762−10764. (b) Damas, A.; Ventura, B.; Moussa, J.; Degli Esposti, A.; Chamoreau, L. M.; Barbieri, A.; Amouri, H. *Inorg. Chem.* **2012**, *51*, 1739−1750. (c) Damas, A.; Gullo, M. P.; Rager, M. N.; Jutand, A.; Barbieri, A.; Amouri, H. *Chem. Commun.* **2013**, *49*, 3796−3798.
(17) Kumar, L.; Puthraya, K. H.; Srivastava, T. S. *Inorg. Chim. Acta* **1984**, *86*, 173−178.
(18) Kamath, S. S.; Uma, V.; Srivastava, T. S. *Inorg. Chim. Acta* **1989**, *166*, 91−98.
(19) Paw, W.; Cummings, S. D.; Mansour, M. A.; Connick, W. B.; Geiger, D. K.; Eisenberg, R. *Coord. Chem. Rev.* **1998**, *171*, 125−150.
(20) (a) Gullo, M. P.; Seneclauze, J. B.; Ventura, B.; Barbieri, A.; Ziessel, R. *Dalton Trans.* **2013**, *42*, 16818−16828. (b) Ventura, B.; Barbieri, A.; Barigelletti, F.; Batcha Seneclauze, J.; Retailleau, P.; Ziessel, R. *Inorg. Chem.* **2008**, *47*, 7048−7058. (c) Ventura, B.; Barbieri, A.; Barigelletti, F.; Diring, S.; Ziessel, R. *Inorg. Chem.* **2010**, *49*, 8333−8346. (d) Williams, J. A. G. *Top. Curr. Chem.* **2007**, *281*, 205−268.
(21) (a) Bauernschmitt, R.; Ahlrichs, R. *Chem. Phys. Lett.* **1996**, *256*, 454−464. (b) Casida, M. E.; Jamorski, C.; Casida, K. C.; Salahub, D. R. *J. Chem. Phys.* **1998**, *108*, 4439−4449. (c) Stratmann, R. E.; Scuseria, G. E.; Frisch, M. J. *J. Chem. Phys.* **1998**, *109*, 8218−8224.
(22) (a) Foster, J. P.; Weinhold, F. *J. Am. Chem. Soc.* **1980**, *102*, 7211−7218. (b) Reed, A. E.; Curtiss, L. A.; Weinhold, F. *Chem. Rev.* **1988**, *88*, 899−926. (c) Reed, A. E.; Weinstock, R. B.; Weinhold, F. *J. Chem. Phys.* **1985**, *83*, 735−746.
(23) Duisenberg, A. J. M.; Kroon-Batenburg, L. M. J.; Schreurs, A. M. M. *J. Appl. Crystallogr.* **2003**, *36*, 220−229.
(24) Farrugia, L. J. *J. Appl. Crystallogr.* **1999**, *32*, 837−838.
(25) Altomare, A.; Cascarano, G.; Giacovazzo, C.; Guagliardi, A.; Burla, M. C.; Polidori, G.; Camalli, M. *J. Appl. Crystallogr.* **1994**, *27*, 435−436.
(26) Sheldrick, G. M. *Acta Crystallogr., Sect. A* **2008**, *64*, 112−122.
(27) Putz, H.; Brandenburg, K. *Diamond;* Crystal Impact GbR: Bonn, Germany.
(28) (a) Adamo, C.; Barone, V. *J. Chem. Phys.* **1999**, *110*, 6158−6170. (b) Adamo, C.; Scuseria, G. E.; Barone, V. *J. Chem. Phys.* **1999**, *111*, 2889−2899.
(29) Frisch, M. J.; Trucks, G. W.; Schlegel, H. B.; Scuseria, G. E.; Robb, M. A.; Cheeseman, J. R.; Scalmani, G.; Barone, V.; Mennucci, B.; Petersson, G. A.; Nakatsuji, H.; Caricato, M.; Li, X.; Hratchian, H. P.; Izmaylov, A. F.; Bloino, J.; Zheng, G.; Sonnenberg, J. L.; Hada, M.; Ehara, M.; Toyota, K.; Fukuda, R.; Hasegawa, J.; Ishida, M.; Nakajima, T.; Honda, Y.; Kitao, O.; Nakai, H.; Vreven, T.; Montgomery, J. A. J.; Peralta, J. E.; Ogliaro, F.; Bearpark, M.; Heyd, J. J.; Brothers, E.; Kudin, K. N.; Staroverov, V. N.; Kobayashi, R.; Normand, J.; Raghavachari, K.; Rendell, A.; Burant, J. C.; Iyengar, S. S.; Tomasi, J.; Cossi, M.; Rega, N.; Millam, N. J.; Klene, M.; Knox, J. E.; Cross, J. B.; Bakken, V.; Adamo, C.; Jaramillo, J.; Gomperts, R.; Stratmann, R. E.; Yazyev, O.; Austin, A. J.; Cammi, R.; Pomelli, C.; Ochterski, J. W.; Martin, R. L.; Morokuma, K.; Zakrzewski, V. G.; Voth, G. A.; Salvador, P.; Dannenberg, J. J.; Dapprich, S.; Daniels, A. D.; Farkas, Ö.; Foresman, J. B.; Ortiz, J. V.; Cioslowski, J.; Fox, D. J. *Gaussian 09,* Revision A.1; Gaussian, Inc.: Wallingford CT, 2009.
(30) Peterson, K. A.; Figgen, D.; Dolg, M.; Stoll, H. *J. Chem. Phys.* **2007**, *126*, 124101.
(31) Figgen, D.; Peterson, K. A.; Dolg, M.; Stoll, H. *J. Chem. Phys.* **2009**, *130*, 164108.
(32) (a) Hehre, W. J.; Ditchfield, R.; Pople, J. A. *J. Chem. Phys.* **1972**, *56*, 2257−2261. (b) Hariharan, P. C.; Pople, J. A. *Theor. Chim. Acta* **1973**, *28*, 213−222.
(33) Tomasi, J.; Mennucci, B.; Cammi, R. *Chem. Rev.* **2005**, *105*, 2999−3093.
(34) Allouche, A. R. *J. Comput. Chem.* **2011**, *32*, 174−182.
(35) Montalti, M.; Credi, A.; Prodi, L.; Gandolfi, M. T. *Handbook of Photochemistry,* 3rd ed.; CRC Press, Taylor & Francis: Boca Raton, FL, 2006.